

## Article

# Inter- and Intra-Hydrogen Bonding Strategy to Control the Fluorescence of Acylhydrazone-Based Conjugated Microporous Polymers and Their Application to Nitroaromatics Detection

Inhwan Cha <sup>1,†</sup>, Seohyun Baek <sup>1,†</sup>, Sun Gu Song <sup>1</sup>, Junggong Kim <sup>2</sup>, Ho Keun Lee <sup>2</sup>, Jongman Lee <sup>2</sup>,  
Kyung-su Kim <sup>3,\*</sup> and Changsik Song <sup>1,\*</sup> 

<sup>1</sup> Department of Chemistry, Sungkyunkwan University, 2066 Seobu-ro, Jangan-gu, Suwon-si 16419, Korea; playlife@skku.edu (I.C.); backgo04@gmail.com (S.B.); mukhon12@naver.com (S.G.S.)

<sup>2</sup> PNL Global Co., Ltd., B1, 10 Sapyeongdae-ro 2-gil, Seocho-gu, Seoul 06652, Korea; chriskim.kr@gmail.com (J.K.); hokeunlee@hotmail.com (H.K.L.); citycamp8@naver.com (J.L.)

<sup>3</sup> Convergence Research Center for Energy and Environmental Sciences, Sungkyunkwan University, 2066 Seobu-ro, Jangan-gu, Suwon-si 16419, Korea

\* Correspondence: kimkyungsu@skku.edu (K.-s.K.); songcs@skku.edu (C.S.)

† These authors contributed equally to this work.

**Abstract:** Acylhydrazone-based fluorescent conjugated microporous polymers (CMPs) with inter- and intra-hydrogen bonding-controlled emissive properties were prepared. The synthesized CMPs (**BH-CMP** and **ABH-CMP**) were characterized by Fourier-transform infrared spectroscopy, X-ray diffraction, solid-state <sup>13</sup>C cross polarization/magic angle spinning nuclear magnetic resonance spectroscopy, and photoluminescence spectroscopy. Interestingly, **BH-CMP** exhibited emission enhancement via adsorption of water molecules, whereas the emission of **ABH-CMP**, which possesses free amine groups, decreased upon the addition of water molecules. The differences in the emission trends of **BH-CMP** and **ABH-CMP** in the presence of water molecules originate from the formation of different hydrogen-bonding networks in each CMP. The acylhydrazone-based CMPs were applied to the detection of nitroaromatic compounds. As a result, **ABH-CMP** in DMF exhibited high selectivity for 1,3,5-trinitrotoluene (TNT) over other nitroaromatic compounds nitrobenzene, 1-chloro-4-nitrobenzene, 2,3-dichloronitrobenzene, and 2,4-dinitrotoluene.

**Keywords:** aggregation-induced emission; polymorphism; conjugated microporous polymers; nitroaromatic compounds



**Citation:** Cha, I.; Baek, S.; Song, S.G.; Kim, J.; Lee, H.K.; Lee, J.; Kim, K.-s.; Song, C. Inter- and Intra-Hydrogen Bonding Strategy to Control the Fluorescence of Acylhydrazone-Based Conjugated Microporous Polymers and Their Application to Nitroaromatics Detection. *Macromol* **2021**, *1*, 234–242. <https://doi.org/10.3390/macromol1030016>

Academic Editor: Angels Serra

Received: 9 August 2021

Accepted: 1 September 2021

Published: 15 September 2021

**Publisher's Note:** MDPI stays neutral with regard to jurisdictional claims in published maps and institutional affiliations.



**Copyright:** © 2021 by the authors. Licensee MDPI, Basel, Switzerland. This article is an open access article distributed under the terms and conditions of the Creative Commons Attribution (CC BY) license (<https://creativecommons.org/licenses/by/4.0/>).

## 1. Introduction

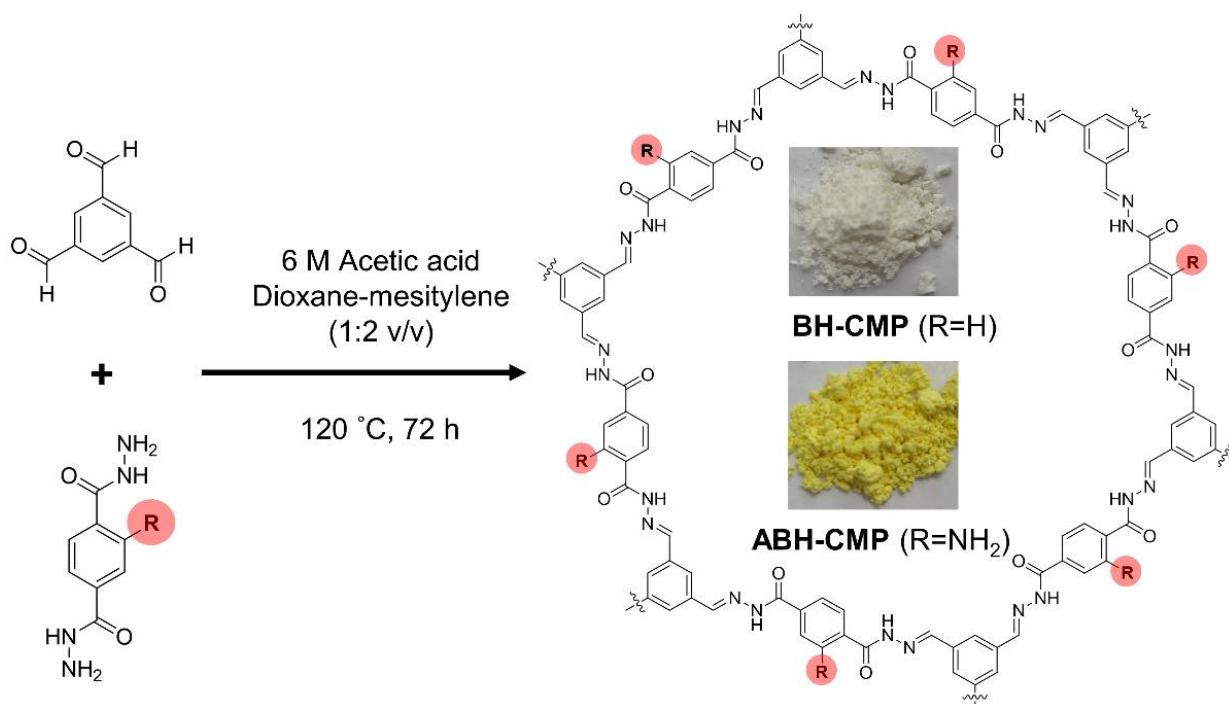
Aggregation-induced emission luminogens (AIEgens) have been intensively applied in optoelectronics such as organic light-emitting diodes (OLEDs) [1–7], sensors [8,9], and bio-imaging [10–12]. Most organic luminogens exhibit lower fluorescence in the solid-state than in the liquid state via a nonradiative decay pathway due to the occurrence of strong  $\pi$ - $\pi$  interactions in the solid state, whereas AIEgens emit strongly in the solid-state. The possible mechanisms of emission of AIEgens mainly include *J*-aggregate formation [13,14], twisted intramolecular charge transfer [15,16], and restriction of intramolecular motions (RIM) [17,18], among which the latter has been most commonly proposed. In a previous study, we discovered that the solid-state emission of bis-arylacylhydrazone (BAH)-based luminogens can be turned on and off by reversible adsorption of water vapors, which enabled the fabrication of rewritable papers with “water-ink” [19]. Specifically, we found that the formation of interlayer hydrogen-bonding networks in the presence of water results in parallel *J*-type aggregates with planarization, thereby enhancing the fluorescence. In other words, we proposed that the fluorescence in BAH is caused by water-specific polymorphism-induced emission enhancement (PIEE) instead of by RIM. However, to

confirm this hypothesis, an analysis in network polymer systems with significantly limited intramolecular motion rather than in a single molecule is required.

Conjugated microporous polymers (CMPs) are a class of porous network polymers that have nanopores and  $\pi$ -conjugated skeletons [20,21]. CMPs are attractive candidates as chemosensory materials because of their large surface area, which provides numerous interaction sites for analyte recognition [22,23]. For example, Geng et al. reported that benzoquinone-based CMPs showed a highly sensitive fluorescence quench by picronic acid [24]. Liu et al. developed a highly luminescent carbazole-based CMP that works as a fluorescent chemosensor toward nitroaromatic compounds (NACs) such as nitrobenzene (NB), 2-nitrotoluene, and 2,4-dinitrotoluene (DNT) [25]. Notably, the detection of NACs is essential for the environment and national security because of their explosiveness and toxicity [26,27].

To construct CMPs, various linkages have been intensively used, including boroxine [28,29], boronic ester [30], imine [31], azine [32], imide [33], and hydrazone [34]. Among them, hydrazone linkages are effective candidates for the construction of CMP building blocks with synthetic accessibility [35] and stimuli responsiveness [36]. Loh et al. reported acylhydrazone-based 2-dimensional covalent organic frameworks (COFs) with tunable solid-state photoluminescence (PL) via interlayer and intralayer hydrogen bonds [37]. They attributed the origin of emission of the acylhydrazone-based COFs to the restriction of intramolecular rotation (RIR) mechanism. However, we previously showed that the emission of BAH moieties occurs not by RIR but by planarization and formation of *J*-aggregates [19]. Thus, to gain more insight into the origin of the emission in BAH, we were interested in investigating network polymer systems by introducing acylhydrazone into CMPs with limited intramolecular motion.

Herein, we report novel acylhydrazone-based fluorescent CMPs with and without intramolecular hydrogen-bond donors (Scheme 1). We investigated the origin of emissive behaviors of the acylhydrazone-based CMPs, which are in a state of minimal intramolecular motions. In particular, we studied the effect of the water-induced hydrogen-bonding pattern on the luminescence properties of the CMPs. Furthermore, the synthesized fluorescent CMPs were utilized for the detection of NACs, including 1,3,5-trinitrotoluene (TNT).



**Scheme 1.** Synthesis of acylhydrazone-based fluorescent conjugated microporous polymers (CMPs) via acetic acid-catalyzed hydrazone formation reaction.

## 2. Experimental Section

### 2.1. Materials

2-Aminoterephthalic-1,4-terephthaloylhydrazide [38] and TNT [39] were synthesized following previously reported procedures. 1,3,5-Triformylbenzene was purchased from Acros Organics (Geel, Belgium). Terephthalic dihydrazide was purchased from Alfa Aesar (Ward Hill, MA, USA). Nitrobenzene (NB) was purchased from Junsei Chemical Co., Ltd. (Tokyo, Japan). 2,3-Dichloronitrobenzene (DCNB) was purchased from Tokyo Chemical Industry CO., Ltd. (Tokyo, Japan). 1-Chloro-4-nitrobenzene (CNB) and DNT were purchased from Sigma-Aldrich (St. Louis, MO, USA). Dimethylformamide (DMF), tetrahydrofuran (THF), *N*-methyl-2-pyrrolidone (NMP), dioxane, mesitylene, acetic acid (AcOH) were purchased from Samchun Pure Chemical Co., Ltd. (Seoul, Korea). All the chemicals were used as received without further purification.

### 2.2. Instruments

PL spectra were recorded on a FluoroMate FS-2 fluorescence spectrophotometer (SCINCO, Seoul, Korea) under constant measurement conditions (500 V PMT voltage, 10 nm slit width, and  $\lambda_{\text{ex}} = 330$  nm, room temperature). Fourier transform infrared (FTIR) spectra were recorded using a VERTEX 70 spectrometer equipped with a diamond-attenuated total reflection (ATR) unit (Bruker Optics Inc., Ettlingen, Germany). Powder X-ray diffraction (PXRD) patterns were obtained using a Rigaku Ultima IV device with a Cu  $K_{\alpha}$  X-ray source (Rigaku Co., Ltd., Tokyo, Japan). Solid-state  $^{13}\text{C}$  cross-polarization/magic-angle spinning nuclear magnetic resonance (CP/MAS NMR) spectra were recorded on a 500 MHz solid-state NMR spectrometer (AVANCE III HD, Bruker, Germany) at the National Center for Inter-University Research Facilities (NCIRF) at Seoul National University.

### 2.3. Synthesis

**Synthesis of BH-CMP.** BH-CMP was synthesized via the AcOH-catalyzed reversible condensation reaction. Briefly, a 10 mL Pyrex tube was charged with 1,3,5-triformylbenzene (0.1 g, 0.62 mmol), terephthalic dihydrazide (0.18 g, 0.93 mmol), dioxane (1.5 mL), mesitylene (3.0 mL), and AcOH (0.5 mL, 6 M). The mixture was sonicated for 5 min, degassed under vacuum, and then heated at 120 °C for 3 days to afford white powder. To remove the starting material and solvent, the product was centrifuged, and washed with THF and NMP. Yield: 0.23 g (82%).

**Synthesis of ABH-CMP.** ABH-CMP was obtained as a yellow powder following the same method as described above for the synthesis of BH-CMP using 1,3,5-triformylbenzene (0.1 g, 0.62 mmol) and 2-aminoterephthalic-1,4-terephthaloylhydrazide (0.19 g, 0.93 mmol). Yield: 0.25 g (85%).

### 2.4. PL Measurements

A 1.0 mg portion of the CMPs was added into 1 mL of a H<sub>2</sub>O/DMF solvent mixture. The resulting mixture was sonicated for 10 min for dispersion. Then, the PL of the CMP suspension was measured by adding a concentrated solution of NACs until the intensity of the PL signal decreased by at least 70% of the initial PL intensity at maximum emission wavelength (BH-CMP 60: 470 nm, ABH-CMP 0: 478 nm, ABH-CMP 60: 486 nm) upon excitation at 330 nm with exposure for 50 ms at room temperature.

## 3. Results and Discussion

We found in our previous work that the emission of the BAH moiety is enhanced by planarization and *J*-aggregation induced by water-specific polymorphism rather than by the RIM mechanistic pathway exclusively [19], which led us to introduce the arylacylhydrazone into a CMP to obtain minimal intramolecular motion. We designed two types of acylhydrazone-based CMPs, i.e., with and without intramolecular hydrogen-bond donors (Scheme 1).

Thus, 2-aminoterephthalic-1,4-terephthaloylhydrazide was chosen as the building block for introducing intramolecular hydrogen bonding into the CMP, and terephthalic dihydrazide was selected to prepare a CMP without intramolecular hydrogen bonding. The acylhydrazone-based CMPs were easily synthesized via the AcOH-catalyzed hydrazone formation reaction between 1,3,5-triformylbenzene and terephthalic dihydrazide (**BH-CMP**) or 2-aminoterephthalic-1,4-terephthaloylhydrazide (**ABH-CMP**). In the FTIR spectra, the imine (C=N) stretching bands of **BH-CMP** and **ABH-CMP** were observed at 1624 and 1616  $\text{cm}^{-1}$ , respectively (Figure S1). In addition, the free amine contained in **ABH-CMP** showed an N–H stretching mode at around 3300  $\text{cm}^{-1}$ , whereas a similar peak was not observed for **BH-CMP**. The solid-state  $^{13}\text{C}$  CP/MAS NMR spectra of **BH-CMP** and **ABH-CMP** revealed the presence of the carbonyl group (C=O), which gave rise to signals in the 192–199 ppm range (Figure S2), and the signal from the C=N group at 167 ppm supports the formation of an acylhydrazone bond. The PXRD patterns of **BH-CMP** and **ABH-CMP** exhibited both sharp and broad features, which indicates the coexistence of amorphous and crystalline components (Figure S3).

To investigate the emission properties of **BH-CMP** and **ABH-CMP**, we measured the water fraction-dependent PL emission spectra for **BH-CMP** and **ABH-CMP** (Figure 1). Initially, a **BH-CMP** dispersion in DMF (1.0 mg/mL) was non-emissive, whereas **ABH-CMP** dispersed in DMF exhibited bright blue emission at 478 nm. Upon increasing the water fraction in the water/DMF cosolvent system containing **BH-CMP** (from 0% to 60%, Figure 1a), a central emission band appeared at approximately 470 nm with full width at half-maximum (FWHM) of 108 nm and increased gradually. However, the addition of water beyond the water fraction of 60% led to a slight decrease in the emission intensity due to the poor dispersibility of the water/DMF cosolvent causing precipitation (Figure 1b). Notably, this emission enhancement occurred in a network polymer system, which is already “aggregated”, indicating that the emission of the acylhydrazone moiety is induced by water-specific polymorphism and not by RIM.

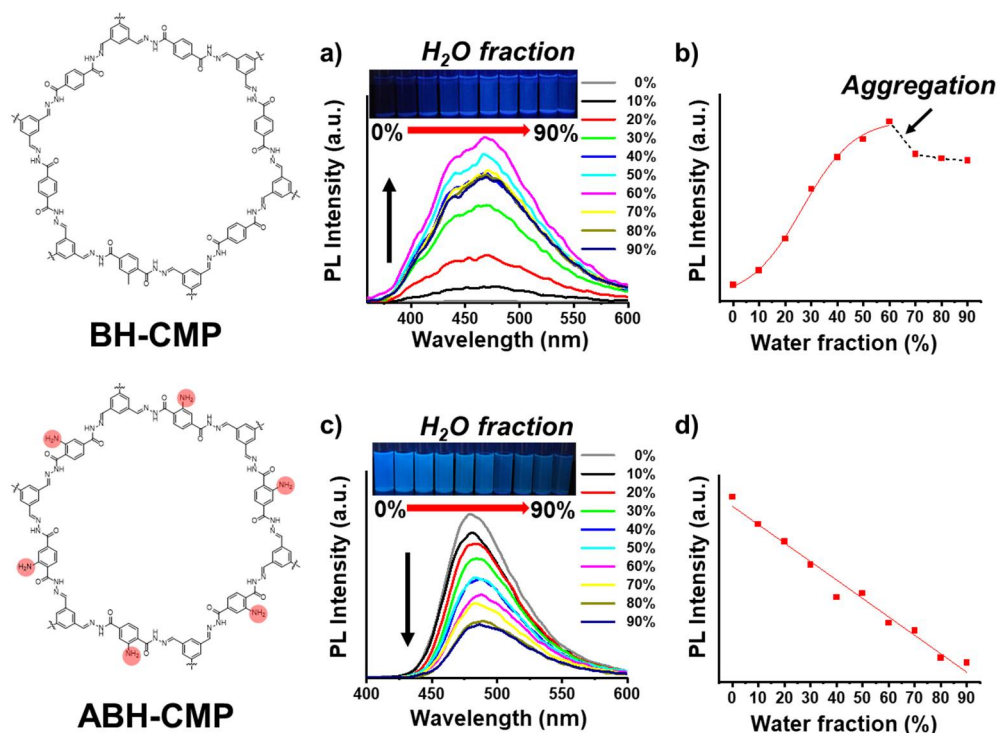


**Figure 1.** Photoluminescence (PL) emission spectra of (a) **BH-CMP** and (c) **ABH-CMP** in a water/DMF dispersion (1.0 mg/mL, water/DMF ratios of 0:10–9:1) (inset: images of **BH-CMP** and **ABH-CMP** under a 365 nm ultraviolet lamp). Plots of the PL intensity of (b) **BH-CMP** and (d) **ABH-CMP** versus the water fraction in a water/DMF dispersion.

Alternatively, the water fraction-dependent PL emission spectra of **ABH-CMP** showed a different pattern from that of **BH-CMP**. Upon increasing the water fraction in the water/DMF mixture containing **ABH-CMP** from 0% to 90%, the maximum emission band that initially appeared at 478 nm with FWHM of 63 nm showed a bathochromic shift ( $\sim 10$  nm), and the emission intensity gradually decreased. This red-shift in the PL emission spectra possibly originated from the change in the microenvironment of the chromophore in **ABH-CMP**. It is noteworthy that with the increase of the water fraction, the fluorescence emission was enhanced in the case of **BH-CMP**, whereas the fluorescence emission gradually decreased for **ABH-CMP**.

Figure 2 depicts a possible mechanism for the two different phenomena. The intramolecular rotation of the central benzene of **BH-CMP** can occur weakly even in the crystalline phase (Figure 2a), causing a non-radiative decay. After adding water molecules to the **BH-CMP** dispersion, the carbonyl oxygen and amide proton in **BH-CMP** are locked via intermolecular hydrogen bonding. Furthermore, this hydrogen bonding induces the planarization and formation of *J*-aggregates, resulting in water-specific PIEE [19]. Unlike **BH-CMP**, **ABH-CMP** exhibits a planar conformation due to intramolecular hydrogen bonding between the amine group on the central benzene and the carbonyl oxygen (Figure 2b). This intramolecular hydrogen bonding can block the non-radiative decay pathway induced by RIM, resulting in **ABH-CMP** emitting fluorescence even in the absence of water molecules. In contrast, after adsorption of water molecules, the planarized and fluorescent **ABH-CMP** is distorted and disaggregated due to disruption of the intramolecular hydrogen bonding, resulting in fluorescence quenching. This result demonstrates that planarization and *J*-aggregate formation play a decisive role in the emission of acylhydrazone-based CMPs.

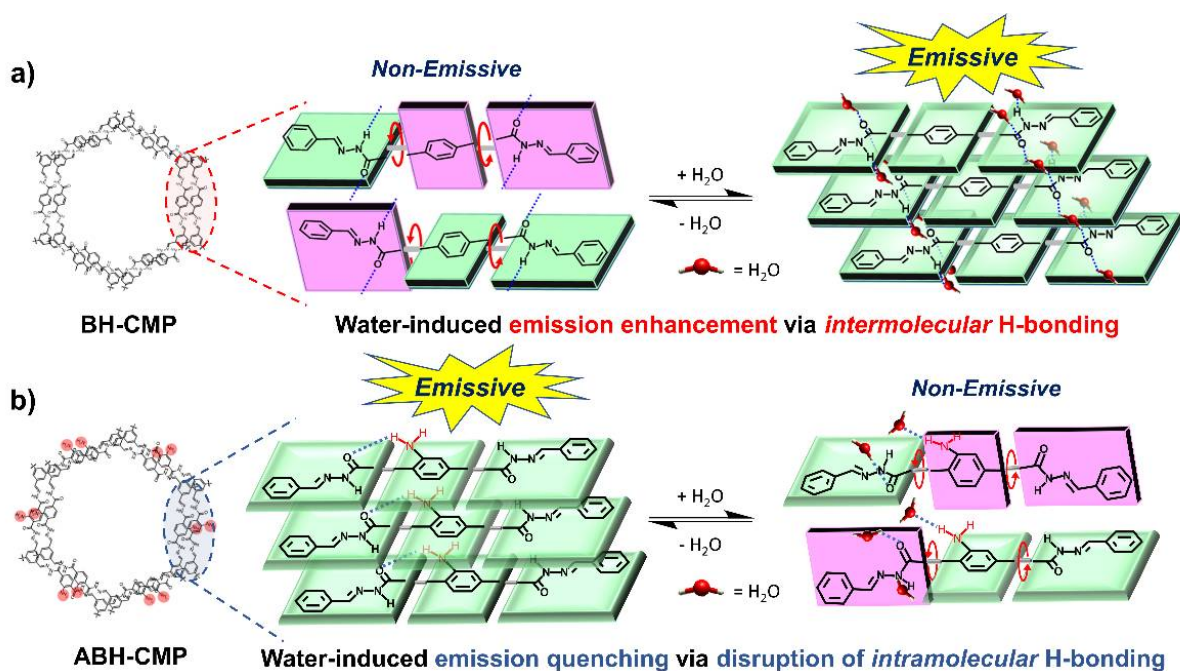


**Figure 2.** Schematic representation of the proposed mechanism for water-induced fluorescence regulation. (a) Emission enhancement in **BH-CMP** via intermolecular hydrogen bonding with water molecules; (b) Emission quenching in **ABH-CMP** via disruption of intramolecular hydrogen bonding by water molecules.

Generally, NACs have an electron-deficient planar benzene ring due to the presence of a nitro ( $NO_2$ ) group and can easily form a donor–acceptor complex with an electron-rich aromatic substance [40]. During complexation, the PL in electron-donor aromatic groups is quenched because an electron in the excited state moves to the  $\pi^*$ -orbital of the NACs instead of to the ground state of the donor molecules [41]. **BH-CMP** and **ABH-CMP**, which contain electron-rich and photo-luminous acylhydrazone, seem suitable for the detection

of NACs. Therefore, we investigated the fluorescence detection ability of **ABH-CMP** and **BH-CMP** for various NACs, including the well-known explosive material TNT.

After dispersing **BH-CMP** and **ABH-CMP** at 1 mg/mL in the 60% H<sub>2</sub>O/DMF mixture in which **BH-CMP** shows the highest PL intensity, a TNT concentration-dependent quenching effect was observed. Thus, the emission of a **BH-CMP** suspension in 60% H<sub>2</sub>O/DMF (**BH-CMP 60**) was almost quenched at a TNT concentration of 1.7 mM, but an **ABH-CMP** suspension in 60% H<sub>2</sub>O/DMF (**ABH-CMP 60**) was quenched at a TNT concentration 2.8 times higher (4.8 mM) (Figure 3a,b). In contrast, the quenching concentration of TNT in an **ABH-CMP** suspension in DMF solvent (**ABH-CMP 0**) was 1.5 mM, which is similar to that of **BH-CMP** (Figure 3c). This result indicates that **ABH-CMP** does not form donor–acceptor complexes with TNT in an H<sub>2</sub>O/DMF co-solvent system.

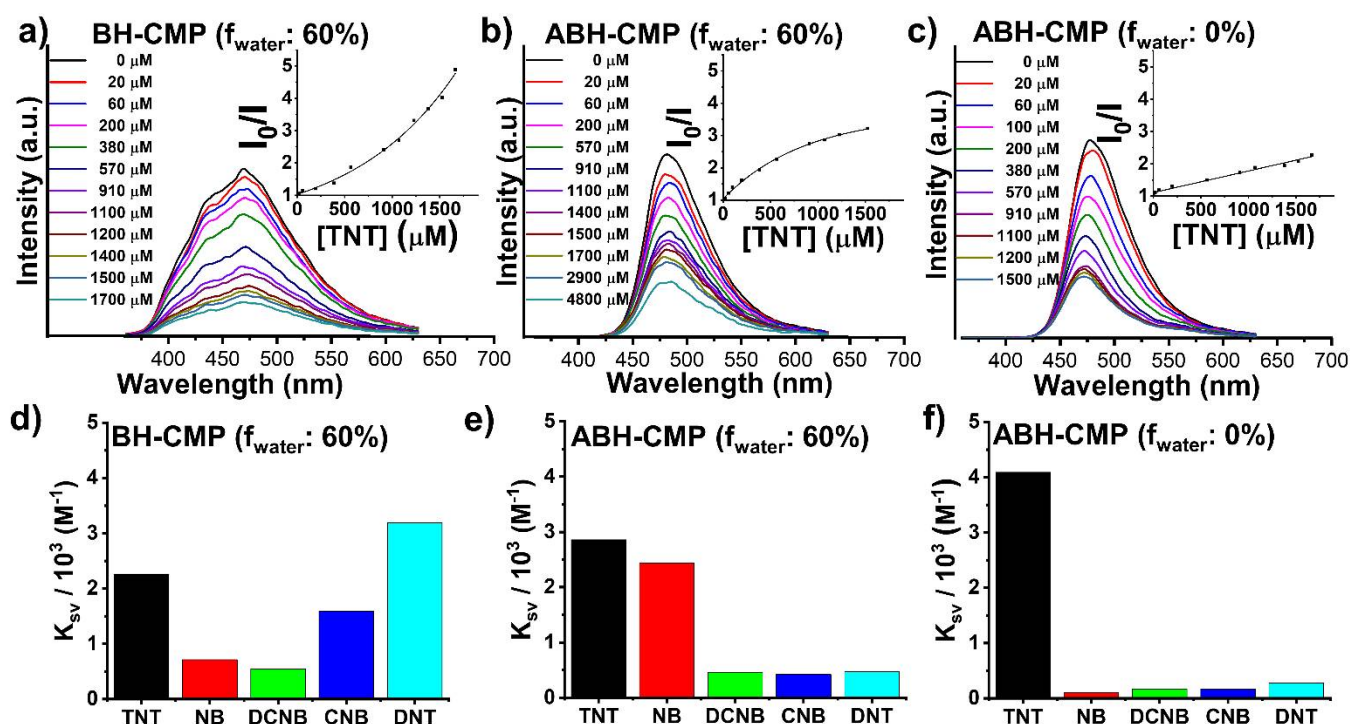


**Figure 3.** Photoluminescence (PL) emission spectra of (a) **BH-CMP 60**, (b) **ABH-CMP 60**, and (c) **ABH-CMP 0** with different concentrations of 1,3,5-trinitrotoluene (TNT). The plots of relative PL intensity ( $I_0/I$ ) of **BH-CMP 60**, **ABH-CMP 60**, and **ABH-CMP 0** versus TNT concentrations are provided as the inset plots ( $I$  = PL intensity,  $I_0$  = PL intensity at a TNT concentration of 0 M). Stern-Volmer constants with TNT, NB, DCNB, CNB, and DNT for (d) **BH-CMP 60**, (e) **ABH-CMP 60**, and (f) **ABH-CMP 0**.

The Stern–Volmer plot of the relative PL intensity of **BH-CMP 60** with different TNT concentrations showed an upward-bent curve, which indicates the occurrence of amplified quenching (Figure 3a, inset) [42]. Moreover, the limit of detection (LOD) of **BH-CMP 60** for TNT was 3.5 μM. The plot of the relative PL quenching intensity of **ABH-CMP 60** versus the TNT concentration was linear, and the LOD for TNT was 29.1 μM, which is higher than that of **BH-CMP 60** (Figure 3b, inset). Unlike **BH-CMP 60**, **ABH-CMP 0**, in which intramolecular hydrogen bonding can be formed, exhibited a downward-bent curve in the Stern–Volmer plot (Figure 3c, inset). At low TNT concentrations, the relative PL intensity of **ABH-CMP 0** for TNT was higher than that of **BH-CMP 60**. However, at higher TNT concentrations, above 1.1 mM, the relative PL intensity of **ABH-CMP 0** for TNT was lower than that of **BH-CMP 60**. The LOD of **ABH-CMP 0** for TNT was 8.8 μM, which was much lower than that of **ABH-CMP 60** but higher than that of **BH-CMP 60**.

We further analyzed the PL quenching concentrations of NACs such as NB, CNB, DCNB, and DNT in **BH-CMP** and **ABH-CMP** suspensions (Figures S4–S6). **BH-CMP**

**60** exhibited PL quenching with a 70% reduction of the initial PL intensity with NAC concentrations ranging from 1.7 mM (TNT) to 5.7 mM (NB), and the LODs of **BH-CMP 60** for NACs were in the range of 3.48  $\mu$ M (TNT) to 213  $\mu$ M (DCNB) (Figure S4 and Table S1). **ABH-CMP 60** showed the same PL reduction in the range of 4.8 mM (TNT) to 15.2 mM (NB), and the LODs of **ABH-CMP 60** for NACs were in the range of 15.3  $\mu$ M (NB) to 201  $\mu$ M (DNT) (Figure S5 and Table S1). Interestingly, according to the Stern–Volmer constants obtained for the NACs (Figure 3f), **ABH-CMP 0** exhibited the highest selectivity for TNT over other NACs. **ABH-CMP 0** exhibited 70% quenching of the initial PL intensity at concentrations between 1.5 mM (TNT) and 17.3 mM (CNB), and the LODs of **ABH-CMP 0** for the NACs were in the range of 2.24  $\mu$ M (DNT) to 408  $\mu$ M (DCNB) (Figure S6 and Table S1). Meanwhile, **BH-CMP 60** showed the highest TNT sensitivity estimated from the LOD; however, its selectivity for NACs was relatively insufficient (Figure 3d). **ABH-CMP 60** showed low sensitivity and poor selectivity for NACs compared with other CMP suspensions (Figure 3e).

#### 4. Conclusions

We synthesized two types of acylhydrazone-based fluorescent CMPs, i.e., **BH-CMP** and **ABH-CMP**, and found that different mechanistic pathways of emission occurred upon adsorption of water molecules, namely, intermolecular hydrogen bonding-induced emission enhancement and emission quenching caused by disruption of intramolecular hydrogen bonding, respectively. The fluorescent **BH-CMP** and **ABH-CMP** were utilized for the sensing of nitroaromatic compounds. The fluorescence emissions of **BH-CMP** and **ABH-CMP** were quenched by photoinduced electron transfer from an excited state of a CMP to the  $\pi^*$  orbitals of NACs including NB, CNB, DCNB, DNT, and TNT. We confirmed the selectivity and sensitivity of **BH-CMP** and **ABH-CMP** suspensions in different solvent systems for NACs by analyzing the LODs and Stern–Volmer constants. An **ABH-CMP** suspension in DMF exhibited high selectivity for TNT over other NACs. We believe that the insight provided in this work offers a new platform for the development of novel fluorescence sensory materials.

**Supplementary Materials:** The following are available online at <https://www.mdpi.com/article/10.3390/macromol1030016/s1>, Figure S1: FT-IR spectra of **BH-CMP** and **ABH-CMP**. Figure S2: Solid-state  $^{13}\text{C}$  CP/MAS NMR of **BH-CMP** and **ABH-CMP**. Figure S3: Powder X-ray diffraction patterns of **BH-CMP** and **ABH-CMP**. Figures S4: The photoluminescence emission spectra of **BH-CMP** suspension in the DMF/H<sub>2</sub>O (40/60; *v/v*) with different concentrations of NACs. Figure S5: The photoluminescence emission spectra of **ABH-CMP** suspension in the DMF/H<sub>2</sub>O (40/60; *v/v*) with different concentrations of NACs. Figure S6: The photoluminescence emission spectra of **ABH-CMP** suspension in the DMF with different concentrations of NACs. Table S1: Limit of Detection of CMPs for NACs.

**Author Contributions:** Conceptualization has been done by J.K., K.-s.K. and C.S. Methodologies were developed by S.B., I.C., S.G.S., H.K.L. and K.-s.K. Writing/editing was done by I.C., J.L., K.-s.K. and C.S. All authors have read and agreed to the published version of the manuscript.

**Funding:** This research has been supported by the Defense Challengeable Future Technology Program of Agency for Defense Development, Republic of Korea. K.-s.K. thanks Korea Initiative for fostering University of Research and Innovation Program of the National Research Foundation (NRF) funded by the Korean government (MSIT) (No. 2020M3H1A1077095).

**Institutional Review Board Statement:** Not applicable.

**Informed Consent Statement:** Not applicable.

**Data Availability Statement:** The data presented in this study are available on request from the corresponding authors.

**Conflicts of Interest:** The authors declare no competing financial interest.

## References

1. Lee, W.W.; Zhao, Z.; Cai, Y.; Xu, Z.; Yu, Y.; Xiong, Y.; Kwok, R.T.; Chen, Y.; Leung, N.L.; Ma, D. Facile access to deep red/near-infrared emissive AIEgens for efficient non-doped OLEDs. *Chem. Sci.* **2018**, *9*, 6118–6125. [[CrossRef](#)] [[PubMed](#)]
2. Chen, B.; Liu, B.; Zeng, J.; Nie, H.; Xiong, Y.; Zou, J.; Ning, H.; Wang, Z.; Zhao, Z.; Tang, B.Z. Efficient Bipolar Blue AIEgens for High-Performance Nondoped Blue OLEDs and Hybrid White OLEDs. *Adv. Funct. Mater.* **2018**, *28*, 1803369. [[CrossRef](#)]
3. Tang, B.Z.; Qin, A. *Aggregation-Induced Emission: Applications*; John Wiley & Sons: Hoboken, NJ, USA, 2013; ISBN 978-1-118-70177-5.
4. Tang, Y.; Tang, B.Z. *Principles and Applications of Aggregation-Induced Emission*; Springer: New York, NY, USA, 2019; ISBN 978-3-319-99037-8.
5. Wurthner, F. Aggregation-Induced Emission (AIE): A Historical Perspective. *Angew. Chem. Int. Ed.* **2020**, *59*, 14192–14196. [[CrossRef](#)]
6. Li, Y.H.; Xu, Z.; Zhu, X.Y.; Chen, B.; Wang, Z.M.; Xiao, B.; Lam, J.W.Y.; Zhao, Z.J.; Ma, D.G.; Tang, B.Z. Creation of Efficient Blue Aggregation-Induced Emission Luminogens for High-Performance Nondoped Blue OLEDs and Hybrid White OLEDs. *ACS Appl. Mater. Inter.* **2019**, *11*, 17592–17601. [[CrossRef](#)] [[PubMed](#)]
7. Wu, D.Y.; Zhang, T.M.; Sun, J.; Wu, Y.L.; Liao, X.Q.; Lu, G.J.; Yang, J.J.; Wang, H.; Li, L.; Xu, B.S. Hyperbranched polymers with aggregation-induced emission property for solution-processed white organic light-emitting diodes. *Tetrahedron* **2018**, *74*, 7218–7227. [[CrossRef](#)]
8. Wang, C.; Li, Q.; Wang, B.; Li, D.; Yu, J. Fluorescent sensors based on AIEgen-functionalised mesoporous silica nanoparticles for the detection of explosives and antibiotics. *Inorg. Chem. Front.* **2018**, *5*, 2183–2188. [[CrossRef](#)]
9. Chen, Y.; Zhang, W.; Cai, Y.; Kwok, R.T.; Hu, Y.; Lam, J.W.; Gu, X.; He, Z.; Zhao, Z.; Zheng, X. AIEgens for dark through-bond energy transfer: Design, synthesis, theoretical study and application in ratiometric Hg<sup>2+</sup> sensing. *Chem. Sci.* **2017**, *8*, 2047–2055. [[CrossRef](#)]
10. Chen, S.; Wang, H.; Hong, Y.; Tang, B.Z. Fabrication of fluorescent nanoparticles based on AIE luminogens (AIE dots) and their applications in bioimaging. *Mater. Horiz.* **2016**, *3*, 283–293. [[CrossRef](#)]
11. Wang, L.; Yang, L.; Cao, D. Application of aggregation-induced emission (AIE) systems in sensing and bioimaging. *Curr. Org. Chem.* **2014**, *18*, 1028–1049. [[CrossRef](#)]
12. Wang, L.; Xia, Q.; Zhang, Z.; Qu, J.; Liu, R. Precise design and synthesis of an AIE fluorophore with near-infrared emission for cellular bioimaging. *Mater. Sci. Eng. C* **2018**, *93*, 399–406. [[CrossRef](#)] [[PubMed](#)]
13. Ma, Z.; Liu, C.; Niu, N.; Chen, Z.; Li, S.; Liu, S.; Li, J. Seeking brightness from nature: J-aggregation-induced emission in cellulosic enzyme lignin nanoparticles. *ACS Sustain. Chem. Eng.* **2018**, *6*, 3169–3175. [[CrossRef](#)]
14. Rodrigues, A.C.B.; de Melo, J.S.S. Aggregation-Induced Emission: From Small Molecules to Polymers—Historical Background, Mechanisms and Photophysics. *Top. Curr. Chem.* **2021**, *379*, 379.
15. Chiang, Y.-C.; Lai, Z.-L.; Chen, C.-M.; Chang, C.-C.; Liu, B. Construction of emission-tunable nanoparticles based on a TICT-AIEgen: Impact of aggregation-induced emission versus twisted intramolecular charge transfer. *J. Mater. Chem. B* **2018**, *6*, 2869–2876. [[CrossRef](#)] [[PubMed](#)]
16. Wang, D.-H.; Chen, L.-J.; Zhao, X.; Yan, X.-P. Enhancing near-infrared AIE of photosensitizer with twisted intramolecular charge transfer characteristics via rotor effect for AIE imaging-guided photodynamic ablation of cancer cells. *Talanta* **2021**, *225*, 122046. [[CrossRef](#)] [[PubMed](#)]
17. Leung, N.L.; Xie, N.; Yuan, W.; Liu, Y.; Wu, Q.; Peng, Q.; Miao, Q.; Lam, J.W.; Tang, B.Z. Restriction of intramolecular motions: The general mechanism behind aggregation-induced emission. *Chem. Eur. J.* **2014**, *20*, 15349–15353. [[CrossRef](#)] [[PubMed](#)]
18. Wang, H.; Zhao, E.; Lam, J.W.; Tang, B.Z. AIE luminogens: Emission brightened by aggregation. *Mater. Today* **2015**, *18*, 365–377. [[CrossRef](#)]
19. Cho, H.J.; Kim, K.-S.; Kim, H.; Kim, T.; Malyutin, A.G.; Rees, D.C.; Yoo, B.-K.; Song, C. Microcrystal Electron Diffraction Elucidates Water-Specific Polymorphism-Induced Emission Enhancement of Bis-Arylacylhydrazones. *ACS Appl. Mater. Int.* **2021**, *13*, 7546–7555. [[CrossRef](#)]
20. Yang, S.-J.; Ding, X.; Han, B.-H. Conjugated microporous polymers with extended  $\pi$ -structures for organic vapor adsorption. *Macromolecules* **2018**, *51*, 947–953. [[CrossRef](#)]
21. Lee, J.-S.M.; Cooper, A.I. Advances in conjugated microporous polymers. *Chem. Rev.* **2020**, *120*, 2171–2214. [[CrossRef](#)]
22. Gao, R.; Zhao, W.; Qiu, Q.; Xie, A.; Cheng, S.; Jiao, Y.; Pan, X.; Dong, W. Fluorescent conjugated microporous polymer (CMP) derived sensor array for multiple Organic/Inorganic contaminants detection. *Sens. Actuators B Chem.* **2020**, *320*, 128448. [[CrossRef](#)]
23. Liu, H.; Wang, Y.; Mo, W.; Tang, H.; Cheng, Z.; Chen, Y.; Zhang, S.; Ma, H.; Li, B.; Li, X. Dendrimer-Based, High-Luminescence Conjugated Microporous Polymer Films for Highly Sensitive and Selective Volatile Organic Compound Sensor Arrays. *Adv. Funct. Mater.* **2020**, *30*, 1910275. [[CrossRef](#)]
24. Geng, T.-M.; Li, D.-K.; Zhu, Z.-M.; Guan, Y.-B.; Wang, Y. The synthesis and fluorescence detection properties of benzoquinone-based conjugated microporous/mesoporous polymers. *Micropor. Mesopor. Mater.* **2016**, *231*, 92–99. [[CrossRef](#)]
25. Zhang, Y.; Sigen, A.; Zou, Y.; Luo, X.; Li, Z.; Xia, H.; Liu, X.; Mu, Y. Gas uptake, molecular sensing and organocatalytic performances of a multifunctional carbazole-based conjugated microporous polymer. *J. Mater. Chem. A* **2014**, *2*, 13422–13430. [[CrossRef](#)]

26. Masunaga, K.; Hayama, K.; Onodera, T.; Hayashi, K.; Miura, N.; Matsumoto, K.; Toko, K. Detection of aromatic nitro compounds with electrode polarization controlling sensor. *Sens. Actuators B Chem.* **2005**, *108*, 427–434. [[CrossRef](#)]
27. Kulkarni, M.; Chaudhari, A. Microbial remediation of nitro-aromatic compounds: An overview. *J. Environ. Manag.* **2007**, *85*, 496–512. [[CrossRef](#)]
28. Cote, A.P.; Benin, A.I.; Ockwig, N.W.; O’Keeffe, M.; Matzger, A.J.; Yaghi, O.M. Porous, crystalline, covalent organic frameworks. *Science* **2005**, *310*, 1166–1170. [[CrossRef](#)]
29. Wang, R.N.; Zhang, X.R.; Wang, S.F.; Fu, G.S.; Wang, J.L. Flatbands in 2D boroxine-linked covalent organic frameworks. *Phys. Chem. Chem. Phys.* **2016**, *18*, 1258–1264. [[CrossRef](#)]
30. Spitler, E.L.; Koo, B.T.; Novotney, J.L.; Colson, J.W.; Uribe-Romo, F.J.; Gutierrez, G.D.; Clancy, P.; Dichtel, W.R. A 2D Covalent Organic Framework with 4.7-nm Pores and Insight into Its Interlayer Stacking. *J. Am. Chem. Soc.* **2011**, *133*, 19416–19421. [[CrossRef](#)]
31. Segura, J.L.; Mancheno, M.J.; Zamora, F. Covalent organic frameworks based on Schiff-base chemistry: Synthesis, properties and potential applications. *Chem. Soc. Rev.* **2016**, *45*, 5635–5671. [[CrossRef](#)]
32. Stegbauer, L.; Hahn, M.W.; Jentys, A.; Savasci, G.; Ochsenfeld, C.; Lercher, J.A.; Lotsch, B.V. Tunable Water and CO<sub>2</sub> Sorption Properties in Isostructural Azine-Based Covalent Organic Frameworks through Polarity Engineering. *Chem. Mater.* **2015**, *27*, 7874–7881. [[CrossRef](#)]
33. Wu, S.F.; Gu, S.; Zhang, A.Q.; Yu, G.P.; Wang, Z.G.; Jian, J.G.; Pan, C.Y. A rational construction of microporous imide-bridged covalent-organic polytriazines for high-enthalpy small gas absorption. *J. Mater. Chem. A* **2015**, *3*, 878–885. [[CrossRef](#)]
34. Stegbauer, L.; Schwinghammer, K.; Lotsch, B.V. A hydrazone-based covalent organic framework for photocatalytic hydrogen production. *Chem. Sci.* **2014**, *5*, 2789–2793. [[CrossRef](#)]
35. Uribe-Romo, F.J.; Doonan, C.J.; Furukawa, H.; Oisaki, K.; Yaghi, O.M. Crystalline Covalent Organic Frameworks with Hydrazone Linkages. *J. Am. Chem. Soc.* **2011**, *133*, 11478–11481. [[CrossRef](#)] [[PubMed](#)]
36. Wang, Y.J.; Liu, Y.Z.; Li, H.; Guan, X.Y.; Xue, M.; Yan, Y.S.; Valtchev, V.; Qiu, S.L.; Fang, Q.R. Three-Dimensional Mesoporous Covalent Organic Frameworks through Steric Hindrance Engineering. *J. Am. Chem. Soc.* **2020**, *142*, 3736–3741. [[CrossRef](#)] [[PubMed](#)]
37. Li, X.; Gao, Q.; Wang, J.F.; Chen, Y.F.; Chen, Z.H.; Xu, H.S.; Tang, W.; Leng, K.; Ning, G.H.; Wu, J.S.; et al. Tuneable near white-emissive two-dimensional covalent organic frameworks. *Nat. Commun.* **2018**, *9*, 2335. [[CrossRef](#)] [[PubMed](#)]
38. Miladinova, P.M.; Konstantinova, T.N. Synthesis and properties of some new blue-emitting triazine derivatives of 2-aminoterephthalic acid, containing a polymerisable group and stabiliser fragment. *Color. Technol.* **2009**, *125*, 242–247. [[CrossRef](#)]
39. Kyprianou, D.; Berglund, M.; Emma, G.; Rarata, G.; Anderson, D.; Diaconu, G.; Exarchou, V. Synthesis of 2,4,6-Trinitrotoluene (TNT) Using Flow Chemistry. *Molecules* **2020**, *25*, 3586. [[CrossRef](#)]
40. Zyryanov, G.V.E.; Kopchuk, D.S.; Kovalev, I.S.; Nosova, E.V.; Rusinov, V.L.; Chupakhin, O.N. Chemosensors for detection of nitroaromatic compounds (explosives). *Russ. Chem. Rev.* **2014**, *83*, 783. [[CrossRef](#)]
41. Skorjanc, T.; Shetty, D.; Valant, M. Covalent Organic Polymers and Frameworks for Fluorescence-Based Sensors. *ACS Sens.* **2021**, *6*, 1461–1481. [[CrossRef](#)]
42. Dong, W.Y.; Pina, J.; Pan, Y.Y.; Preis, E.; de Melo, J.S.S.; Scherf, U. Polycarbazoles and polytriphenylamines showing aggregation-induced emission (AIE) and intramolecular charge transfer (ICT) behavior for the optical detection of nitroaromatic compounds. *Polymer* **2015**, *76*, 173–181. [[CrossRef](#)]